IOP Publishing Environ. Res. Lett. 20 (2025) 074045 https://doi.org/10.1088/1748-9326/ade16e

ENVIRONMENTAL RESEARCH
LETTERS

LETTER

Threefold increase in most intense South Atlantic convergence zone events by 2100 in convection-permitting simulation

Marcia T Zilli[1,*], **Neil C G Hart**[1], **Kate Halladay**[2] **and Ron Kahana**[2]

[1] School of Geography and the Environment, University of Oxford, Oxford OX1 3QY, United Kingdom
[2] Met Office Hadley Centre for Climate Science and Services, Exeter EX1 3PB, United Kingdom
[*] Author to whom any correspondence should be addressed.

E-mail: marcia.zilli@ouce.ox.ac.uk

Keywords: South Atlantic convergence zone, intense precipitation, future precipitation intensification, convection-permitting regional climate model

OPEN ACCESS

RECEIVED
4 February 2025

REVISED
15 April 2025

ACCEPTED FOR PUBLICATION
5 June 2025

PUBLISHED
16 June 2025

Original Content from this work may be used under the terms of the Creative Commons Attribution 4.0 licence.

Any further distribution of this work must maintain attribution to the author(s) and the title of the work, journal citation and DOI.

Abstract

Unprecedented rainfall extremes resulting from global warming are becoming more frequent each year, including over South America. In this region, tropical-extratropical (TE) cloud bands in the South Atlantic convergence zone (SACZ) produce most of the rainy season precipitation. In this study, we diagnose the impacts of warming on the frequency and intensification of SACZ TE cloud bands. The cloud bands are identified using a feature-detection algorithm applied to a suite of convection-permitting simulations produced by the UK Met Office. Intensely raining clusters embedded within these large-scale cloud bands are diagnosed in order to identify the most intense events. Although the total number of cloud-band days will see a 20%–30% decrease in their frequency under high-emission global warming, the present day 1-in-5 most intense cloud-band days will happen every 3-in-5 cloud-band days in the future. Therefore, despite fewer cloud-band days occurring in a given year, when they form they will frequently be more intense than is typical in the current climate. This increase is primarily due to warming-driven intensification of rain rates within the heavily raining clusters embedded in these weather systems. These results highlight the growing risk of intense SACZ rainfall over South America under warming, increasing the likelihood of flash floods, landslides, and unprecedented catchment-scale fluvial flooding.

1. Introduction

Rainfall across most of subtropical South America is dominated by continental-scale tropical-extratropical (TE) cloud bands, known as South Atlantic convergence zone (SACZ) events when persisting for more than 3 days (Zilli and Hart 2021). In Brazil, most of the key agricultural regions and populated cities, including São Paulo and Rio de Janeiro, rely on SACZ events for the majority of their annual rainfall (Zilli and Hart 2021), experiencing droughts in years with few or displaced events (Coelho *et al* 2016). However, risks of flooding and landslides (da Fonseca Aguiar and Cataldi 2021) are greatly increased by SACZ events and intense mesoscale rainfall systems embedded within the continental-scale cloud bands (e.g. deep convection patches within the cloud structure in figure 1). These risks are well understood, but what might happen to the intensity of SACZ-related rainfall as the climate warms?

Across the globe, observed increases in rainfall intensity are associated with a warming atmosphere, generally following Clasius–Claperyon (CC) scaling of $\sim$7% K^{-1}. However, substantial regional variation in these scaling rates are observed and, for sub-daily extreme rainfall, intensification of up to double the CC-scaling has also been observed (Lenderink and van Meijgaard 2008, Fowler *et al* 2021). A growing number of studies demonstrate that to adequately simulate rainfall intensification, convection-permitting climate model (CPM) configurations are required to capture observed trends

© 2025 The Author(s). Published by IOP Publishing Ltd

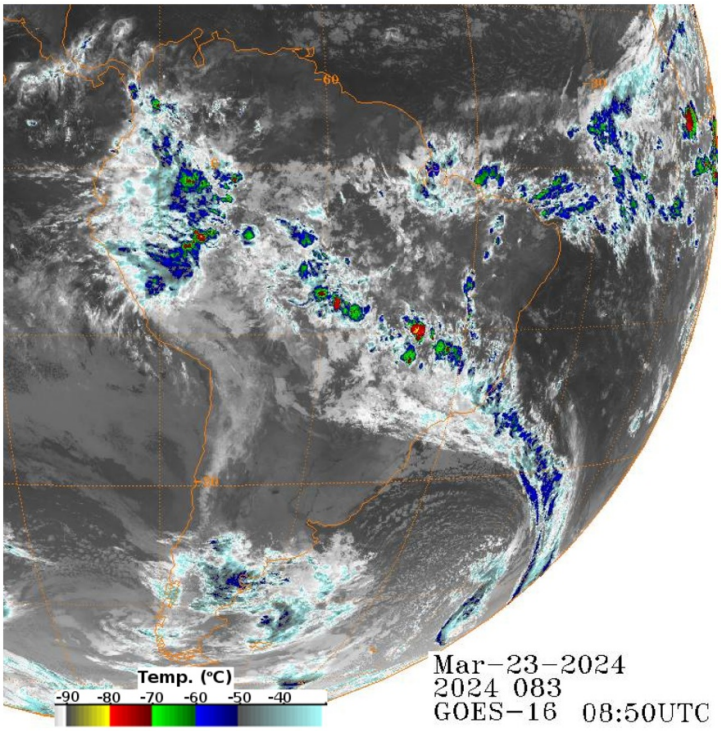

Figure 1. Satellite image of an example tropical-extratropical (TE) cloud band extending from the tropical Amazon rainforest across subtropical South America into the South Atlantic Ocean. Shading indicates cloud top brightness temperature with coldest colour shading indicating deep convection embedded within the cloud band. Courtesy: NOAA-NCEI Global ISCCP B1 Browse System (Knapp 2008).

(Lee *et al* 2022, Lenderink *et al* 2024) and future changes in rainfall intensity (Kendon *et al* 2019).

In this paper, we leverage a suite of Met Office Hadley Centre models of increasing model resolution to diagnose potential changes in the intensity of rainfall within TE cloud bands over South America. TE cloud band events and associated spatial footprints are identified in daily mean outgoing long-wave radiation (OLR) using a feature-detection algorithm developed for and extensively tested on observational and atmospheric model data (Hart *et al* 2012, Zilli and Hart 2021, Zilli *et al* 2023). The suite of models, regardless of horizontal resolution, simulates the annual cycle of TE cloud bands in the region well, with monthly frequencies within 10%–20% of observations (Zilli *et al* 2023). The CPM better simulates intense precipitation on sub-daily (Halladay *et al* 2023) and daily (Zilli *et al* 2024) scales, relative to the driving 25 km convection-parameterised model. Crucially, CPMs are well-documented as better able to represent mesoscale convective organisation (Prein *et al* 2013, Crook *et al* 2019), which may be a key to appropriately simulating intensely raining regions within the TE cloud band (e.g. figure 1) and the potential intensification of rain rates in these regions in the future.

2. Methods

2.1. Data

TE cloud band events and associated spatial footprints are identified in Brazil and parts of South America (study region: 70°–33° W, 40°–0° S) using the daily mean OLR Version 1.2 data set provided by the National Oceanic and Atmospheric Administration Climate Data Record (NOAA CDR; Lee (NOAA-CDR Program) 2011, Lee 2014). The amount of precipitation produced by these events is estimated using the Climate Hazards Center Infrared Precipitation with Station data (CHIRPS; Funk *et al* 2015), a gridded rainfall product obtained by merging satellite imagery and *in-situ* station data. Similar results were also obtained using precipitation from the fifth generation reanalysis of the European Centre for Medium-Range Weather Forecasts (Hersbach *et al* 2020) and the Brazilian daily weather gridded data, a gridded data set based on station-observed precipitation from Brazil (Xavier *et al* 2022).

Here, we examine a suite of convection-permitting regional climate models (CPRCMs) and parameterised simulations produced by the UK Met Office (UKMO). Both present and future simulations have 10 years of data over tropical and subtropical

South America (85°–30° W, 40° S–15° N). The CPRCM simulation uses the Met Office Unified Model (UM) version 10.6 in the atmospheric-only regional configuration (MOHC-HadREM3-RAL1T-4.5 km) using a horizontal grid spacing of 4.5 km, in which deep convection is represented explicitly (i.e. convection parametrization is disabled). The present-day CPRCM simulation (CPRCM-PD) covers the 1998–2007 period and is obtained by directly nesting it in the UKMO atmosphere-only global climate model (MOHC-HadGEM3-GA7GL7, GCM-PD hereafter) run at 25 km horizontal grid spacing (n512 Gaussian grid) with time-varying annual global values of GHG concentration. For a detailed description of the UKMO CPRCM configuration and the present-day simulation, see Halladay *et al* (2023). The future CPRCM simulation (CPRCM-2100), indicative of the climate at the end of the century, also covers 10 years and is forced by a UM simulation similar to that used for CPRCM-PD but now running under the RCP8.5 GHG emissions scenario (CO_2 concentrations fixed at 936 ppm) and sea surface temperatures (SSTs) derived by adding a delta field to present day SSTs. These delta fields are obtained by differencing SST fields from HadGEM2-ES RCP 8.5 simulation between 1975–2005 and 2085–2115 (Reynolds *et al* 2007). The future forcing simulation is referred to as GCM-2100. More details on the configuration of the future simulations are available in Kahana *et al* (2024).

For comparison with results from the Coupled Model Intercomparison Project 6, we also consider the UKMO HadGEM3-GC3.1 (Williams *et al* 2018) historical and future (ssp585) scenarios, at two spatial resolutions: n216 Gaussian grid (n216-H; Andrews *et al* 2020), which equates to a nominal atmospheric resolution of ∼60 km; and n96 (n96-H; Kuhlbrodt *et al* 2018), with nominal atmospheric resolution of ∼135 km. Despite the different configurations (regional versus global) and resolutions (ranging from 135 km in n96-H to 4.5 km in CPRCMs), all simulations are run with the same UM version (Version 10.6).

2.2. Identification of Cloud Band Events

The cloud band events are identified using the automatic feature-detection algorithm described by Hart *et al* (2012) and adapted to South American events by Zilli and Hart (2021). Cloud bands, as identified by the algorithm, are continuous areas with daily average OLR below a threshold, indicative of deep convection, diagonally extending from the tropics to the extratropics. In a previous analysis, Zilli and Hart (2021) compared the cloud band days identified in the NOAA CDR OLR using the feature-detection algorithm to manually-identified SACZ events noted in the operational forecast of the Centre for Weather Forecast and Climatic Studies (CPTEC) of the National Institute for Space Research (INPE) in Brazil. These authors demonstrated that the OLR threshold that results in the closest relationship between these two datasets is 225 $W \cdot m^{-2}$, which we will adopt here.

For simulations, we select the OLR threshold that best reproduces the average number of events identified in the NOAA CDR OLR, which we will refer to as observed events. This step is necessary to account for the positive bias in the OLR simulations (Monerie *et al* 2020, Zilli *et al* 2024). The methodology identifies the OLR threshold necessary to produce a similar number of cloud-band days in each simulation. Despite restricting the number of cloud band days, this approach does not impose the relative monthly frequency and reflects the climatology of each model. More details on the methodology and sensitivity of the results to selected thresholds can be found in Zilli *et al* (2023, 2024). Here, we use the same event-set as in Zilli *et al* (2024) (observed, CPRCM-PD, and GCM-PD datasets) and Zilli *et al* (2023) (n96-H and n216-H), with a chosen threshold of 235 $W \cdot m^{-2}$ for the CPRCM-PD, 240 $W \cdot m^{-2}$ for the GCM-PD, and 245 $W \cdot m^{-2}$ for the n216-H and n96-H simulations. For future projections, we add 10 $W \cdot m^{-2}$ to the present-day OLR threshold of each model to account for the increase in the radiative forcing resulting from the larger CO_2 concentration. This value is roughly equivalent to the increase in OLR in future simulations averaged over the study area.

After identifying the TE cloud band, we calculate the event-related precipitation as the daily precipitation rate over land within the cloud band footprint. These values are averaged over the cloud band land area to produce the area-averaged rainfall rate.

2.3. Selection of Intense Cloud Band Events

First, we calculate the 95th percentile of the area-averaged precipitation rate over the land area of each cloud-band day for each dataset (PP95, considering only areas with precipitation above 1 $mm \cdot d^{-1}$). This is exemplified in the 'Step 1' of figure 2. This metric is equivalent to using the percentiles between 70th and 80th considering the values of all land pixels with precipitation above 1 $mm \cdot d^{-1}$, depending on the dataset/model. Figure 3 (first column) shows the distribution of the area-averaged precipitation rates (histograms) and the PP95 (dashed lines) in each dataset.

The area-averaged rainfall rate does not adequately characterise the most intensely raining mesoscale structures embedded within TE cloud bands, nor potential future increases in these more localised rainfall extremes. These embedded rainfall features are most likely to produce the excessive rainfall associated with flash flooding and landslides.

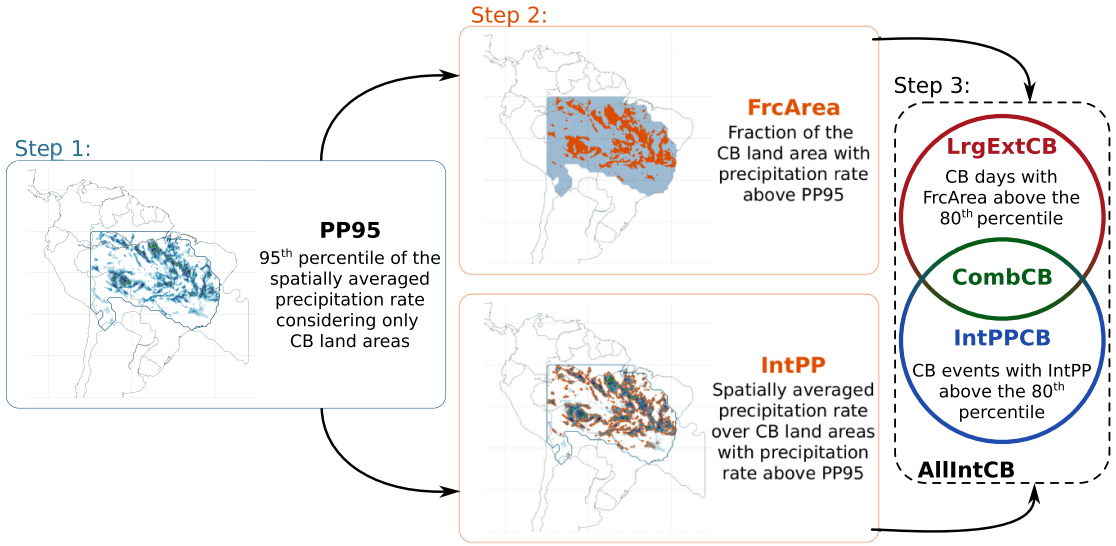

Figure 2. Schematic of the methodology to identify the intense cloud band (CB) events. Step 1 shows how the PP95 threshold is calculated. In step 2, the areas with precipitation above PP95 are identified, resulting in two attributes: the fraction of the cloud band land area with precipitation above the PP95 (FrcArea) and the average precipitation rates over these areas (IntPP). In Step 3, the 80th percentile of these attributes is used to identify the large extent (LrgExtCB), intense precipitation (IntPPCB), and combined (CombCB) intense cloud band events.

So, the next step is to characterise cloud band intensity in terms of these embedded intensely raining regions. To do so, we identify intense rainfall regions within each cloud band as those grid points with rain rates exceeding the present-day PP95. These embedded rain regions can then be characterised both in terms of rainfall rates and spatial extent within the cloud band.

After defining PP95, we calculate two attributes for each cloud band day: the fraction of the cloud band area with precipitation above PP95 (referred to as FrcArea and shaded in orange in the 'Step 2' top map, figure 2) and the spatially-averaged precipitation rate over these areas (IntPP, 'Step 2' bottom map in figure 2). We use these attributes to define two categories of intense cloud band days: large extent cloud band days (LrgExtCB), defined as those days with FrcArea above the 80th percentile (i.e. the top 20% days); and intense precipitation cloud band days (IntPPCB) as those days with IntPP above the 80th percentile ('Step 3' in extended data figure 2). As the same cloud band day can be classified as LrgExtCB and IntPPCB, we define the combined cloud band category (CombCB), representing rarer cloud band days that produce both high intensity and large extent of intense rainfall. The number of cloud-band days in each category is listed in table 1. The distribution of the attributes and their 80th percentile considering all cloud band days in each dataset are summarized in the second and third columns of figure 3.

The choice of 20%, or 1 in 5 cloud band days, ensures a focus on a range of intense rather than very extreme days, which is prudent since the convection-permitting simulations only provide 10 years of data, with ∼100 cloud band days per year. This choice of intense rather than extreme cloud band days also serves an interest in capturing all potentially impactful cloud bands rather than the only most extreme ones. We estimate these metrics for all datasets individually. Since our objective is to evaluate the changes in the frequency and intensity of these cloud band days, we use the simulated present-day values of PP95 and the 80th percentiles of FrcArea and IntPP to identify future intense days.

3. Classification of intense TE cloud band events

First, it is necessary to consider the model fidelity in capturing the core features of the TE cloud band rainfall climatology. In the 1998–2007 period, TE cloud bands are observed on 29% of all days (black dashed line in figure 4(a); numbers also provided in table 1), producing a third (33%, figure 4(c)) of the annual precipitation over the study area, although the contribution varies over space, given the distribution of convective centres within the cloud band (as exemplified in figure 1). Both the driving general circulation atmosphere-only model (GCM-PD) and the CPRCM-PD reproduce the frequency of cloud band days over South America well (blue hatched bars, figure 4(a)). The annual cycle in cloud band frequency, quantified by the fraction of cloud band days occurring in a given month, is well captured across the simulations with increases from near zero in August to a peak of over 60% during the core summer months, from December through February ('All' in figure 4(b); see also Zilli *et al* 2024). Additionally,

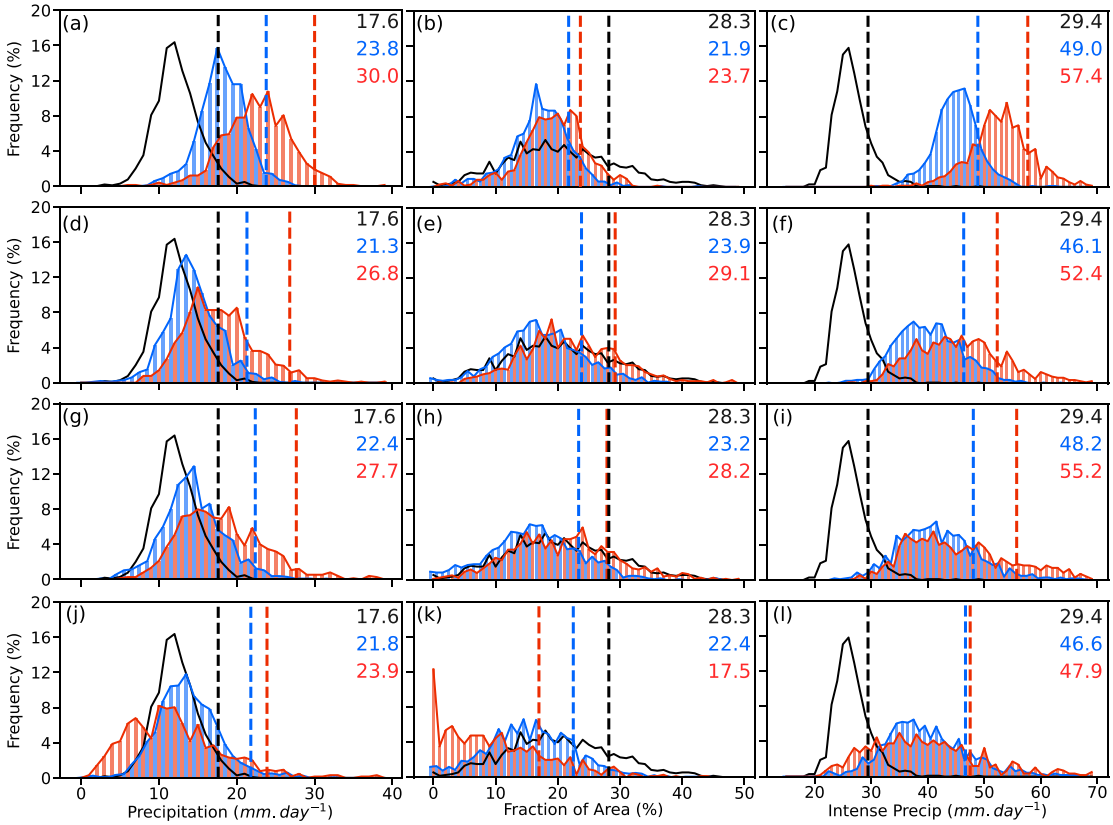

Figure 3. Distribution of the main attributes of each cloud band day: area-averaged precipitation rates (first column), fraction of the cloud band area with intense precipitation (above PP95; second column), and precipitation rate averaged over those areas (third column) for the observed dataset (black lines) and present-day (blue bars) and future (red bars) simulations considering (a)–(c) CPRCM; (d)–(f) GCM; (g)–(i) HadGEM3-GC3.1 n216; and (j)–(l) HadGEM3-GC3.1 n96. In the first column, the dashed lines and values on the top right represent the 95th percentile of the area-averaged precipitation rate (PP95); in the second and third columns, the dashed lines and values represent the 80th of the attributes.

Table 1. Number of cloud band days over the 10-year period (1998–2007) in each dataset, considering all cloud band days (All CB), large extent (LrgExt), intense precipitation (IntPP), and combined (Comb) cloud band days in observations (NOAA CDR) and models.

Model & scenario	All CB	LrgExt	IntPP	Comb
NOAA CDR	1051	210	210	103
CPRCM-PD	992	199	199	81
CPRCM-2100	744	265	599	256
GCM	997	200	200	66
GCM-2100	774	321	370	193
n216-H	1057	212	212	76
n216-ssp585	754	309	295	164
n96-H	1161	232	232	73
n96-ssp585	650	68	139	31

the CPRCM-PD simulates the contribution of cloud band events to total area-averaged annual precipitation most accurately (32%, 'PD' in figure 4(c)), while in the GCM-PD simulation, this value is lower (27%). The spatial distribution of the cloud band days is also well reproduced by the CPRCM-PD, with maximum frequency over the Amazon and extending southeastward along the core SACZ region (figures 5(a) and (b)).

Considering the daily rainfall rate averaged over the TE cloud band area, the CPRCM-PD precipitation distribution is shifted to higher rates than the gridded CHIRPS observations (figure 3(a)), a bias expected from previous studies on CPRCMs (Halladay *et al* 2023, Zilli *et al* 2024). However, the distribution shape matches the observations well, overcoming the skewness bias towards low rain rates typical in parametrised-convection models (Berthou *et al* 2019, Zilli *et al* 2024; see also figures 3(d), (g), and (j)). As Lenderink *et al* (2024) and others (e.g. Lee *et al* 2022) show, convection-permitting models better capture observed scaling of sub-daily rainfall extremes with increased absolute humidity than parametrised-convection models. This indicates that future scaling of intense precipitation under warming may be more accurately estimated by convection-permitting models, despite their present day overly intense rainfall distributions, as seen in figure 3(a). Therefore, we focus here on changes in precipitation obtained by comparing the present and future scenarios, all changes are reported by relative changes in the distribution and in particular the tail of the distribution as captured by its 95th percentile (PP95, dashed lines in figure 3, first column).

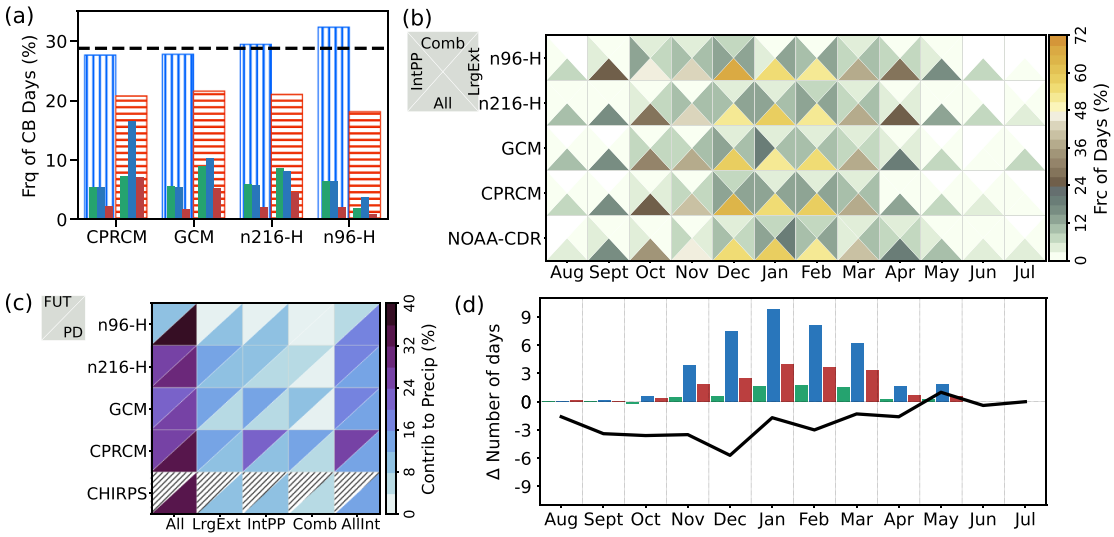

Figure 4. (a) Mean frequency of observed (black dashed line) and simulated cloud band (CB) days in each model, considering the present-day (blue hatched bars) and future (red hatched bars) simulations. The solid bars represent the present and future number of days with large extent (green), intense precipitation (blue), and combined (red) intense CB days. (b) Percentage of cloud band days per month in observations (NOAA-CDR) and all present-day simulations, with each tile representing the values for all (bottom), large extent (right), intense precipitation (left), and combined (top) cloud band days, as represented in the diagram in the top left. (c) Percentage contribution of the cloud bands to the total precipitation, averaged over the cloud band land-area, considering all ('All'), large extent ('LrgExt'), intense precipitation ('IntPP'), combined ('Comb'), and all intense ('AllInt') cloud band days, with each tile representing values in present ('PD', lower right) and future ('FUT', top left) scenarios. (d) Changes in the number of cloud band days per month in the future compared to the present-day simulations, considering all days (bold line), large extent (green bars), intense precipitation (blue bars), and combined (red bars) intense cloud band days.

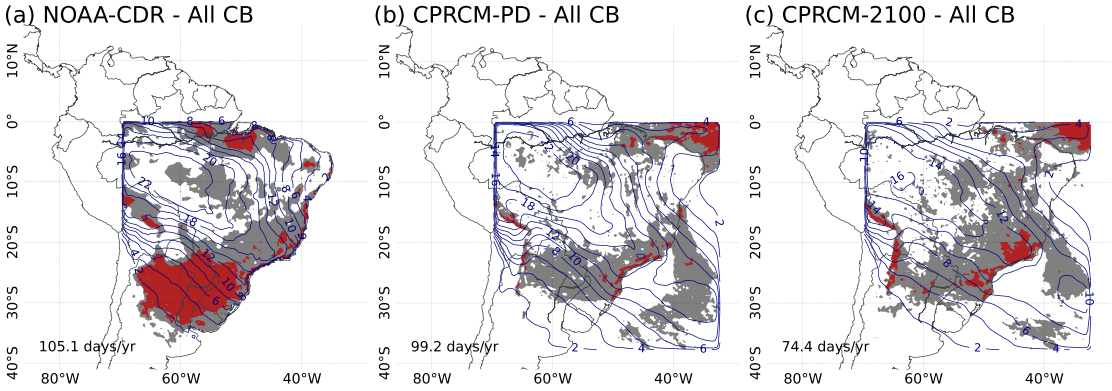

Figure 5. Percentage of days with cloud band (blue contours every 2%) in (a) NOAA-CDR, (b) CPRCM-PD, and (c) CPRCM-2100. Grey (red) shading indicates the areas with more than 20% (30%) of the cloud band days with precipitation above the PP95. The average number of cloud band days per year is indicated on the bottom left of each map.

In the observational dataset (CHIRPS), a typical cloud band has embedded areas of intense rainfall regions covering, on average, 21% of the cloud band land area (FrcArea, figure 3, second column). The CPRCM-PD simulates the observed mean FrcArea well, even though the models overestimate the frequency of CB events with FrcArea between 10% and 23% and underestimate those with FrcArea values exceeding 23% (figure 3(b)). Although the shift in the mean of the FrcArea is marginal in the future CPRCM-2100 simulation (2% increase), there is more than a doubling in the frequency of cloud band days with a larger FrcArea in the upper tail of the distribution (figure 3(b)). Geographically, intense precipitation regions within the cloud band footprint are more frequent over eastern Brazil and Southeastern South America (SESA), where the observed precipitation rate is above PP95 on more than 20% of the cloud band days (grey shades in figure 5(a)). The CPRCM-PD simulation captures the geographical distribution of these events over Southeastern Brazil and parts of SESA, even though it underestimates its relative frequency (figure 5(b)). In the future scenario, the doubled frequency of cloud band days with a

larger FrcArea is reflected geographically by the future expansion of areas in which 1 in 5 (grey) or 1 in 3 (red) cloud band days will produce intense rainfall above PP95, especially across eastern Brazil and the heavily populated southeast coast (figure 5(c)).

As expected from previous analysis of CPRCMs (Halladay *et al* 2023, Zilli *et al* 2024), the simulated distribution of daily rain rates averaged across intensely raining regions (blue, figure 3(c)) is too high in comparison to observed distributions from the gridded data set (black line). Nonetheless, the CPRCM-PD simulation better simulates the distribution of rain rates in intensely raining regions compared to parameterised simulations (figure 3, third column). Importantly, a growing body of evidence indicates that, in spite of the high rain-rate bias of CPRCMs, the observed scaling of intense rainfall with warming is appropriately represented by CPRCMs and poorly represented by convection-parameterised model configurations (Lee *et al* 2022, Lenderink *et al* 2024). Such scaling is clear in figure 3(c) with the mean of the future distribution (red curve) increasing $\sim$10 mm·d^{-1} and the upper tail spanning 60–70 mm·d^{-1} when it barely reached 55 mm·d^{-1} in the present (blue curve). This future increase in intense rain rates is far greater than the increase in fractional area covered by intense rain (figure 3(b)).

4. Warming increases probability of intense events

Figure 3(a) shows a notable increase in the area-average cloud band rain rate in the high-emissions future scenario (CPRCM-2100; shifting from blue to red distributions). In the upper tail of the distribution, PP95 simulated by the CPRCM-PD is 23.8 mm·d^{-1} which increases by 26% to 30.0 mm·d^{-1} in the CPRCM-2100 simulation. The CPRCM-PD PP95 value is equivalent to the 55th-percentile in CPRCM-2100. A similar increase in PP95 is also found in the high-emissions future GCM and n216 fully-coupled simulations (26% and 22%, figures 3(d) and (g), respectively); in the coarser resolution n96 simulation, the increase in PP95 is smaller (10%, figures 3(j)).

Despite the substantial increase in the likelihood of rainfall extremes within the cloud band, the future simulations show a 20%–30% decrease in the frequency of cloud band days (figure 4(a); also table 1), with the largest reduction of 3–6 cloud band days per month between September and December (black line in figure 4(d)). So what is the absolute change in the likelihood of intense cloud bands?

By definition, LrgExtCB and IntPPCB represent each 20% of the total present-day cloud-band days (either observed or simulated), resulting in 19–21 d per calendar year each (5% to 6% of the days; figure 4(a); see also table 1). CombCB days represent $\sim$10% of all observed CB days and occur between 6–10 d per year ($\sim$2% of the days). In total, intense CBs (LrgExtCB + IntPPCB − CombCB) represent 30% of all CB days and are responsible for 40% of the total precipitation produced by all cloud bands, occurring about 30 d per year. All present-day simulations reproduce the observed fraction of intense CB days (figure 4(b)) and their relative contribution to the total precipitation (figure 4(c)).

Under high-emissions end-of-century warming, intense cloud band days become more frequent in all simulations (except n96-ssp585; figure 4(a)). In particular, the CPRCM-2100 simulates 201% more IntPPCB by the end of the century, representing up to 80% of all CB days (figure 4(a)). IntPPCB days, averaging 20 d per year in the CPRCM-PD simulations, are projected to triple in frequency to 60 events annually in 2100. The increase in the number of IntPPCB days also results in an increase in the number of CombCB days (216% in CPRCM-2100; solid red bars in figure 4(a)). In fact, the fraction of LrgExtCB that is also classified as IntPPCB increases from 41% in the present-day to 97% in the CPRCM future scenario, indicating that virtually all LrgExtCB events will also be IntPPCB events (but not the opposite). A similar increase in the ratio of IntPPCB to LrgExtCB is also observed in the parameterised simulations (table 1) as a result of the precipitation intensification. This increase in the frequency of IntPPCB days is most pronounced during the austral summer months NDJFM (blue bars in figure 4(d)).

The contribution of the IntPPCB days to the total annual precipitation increases from 9% in the CPRCM simulation to 24% in the CPRCM-2100 (figure 4(c)). In other words, a quarter of the total precipitation over the study area is projected by the CPRCM model to be produced by IntPPCB days. A similar but less pronounced increase also occurs in the parameterised simulations (except in n96-ssp585). This is in contrast to a decline in the contribution from all events (see first column in figure 4(c)), heightening the relative importance of intense cloud band days. These results suggest that while cloud band events will be rarer in the future when they do occur, they have a substantially higher likelihood of producing intensely raining clusters with these clusters occurring over larger areas than present-day cloud band systems.

Geographically, observed intense cloud band days occur more frequently in the SACZ region (more than 3% of all days for LrgExtCB and IntPPCB and 1% for CombCB, represented by the magenta contour in figure 6, first column). In the subtropics (south of 20° S), intense cloud band days are less frequent (1%–2% of the days or 3–8 d with LrgExtCB or IntPP) but about 50% of them have areas with precipitation above PP95 over the region (figure 6, first column). All simulations reproduce the frequency of intense

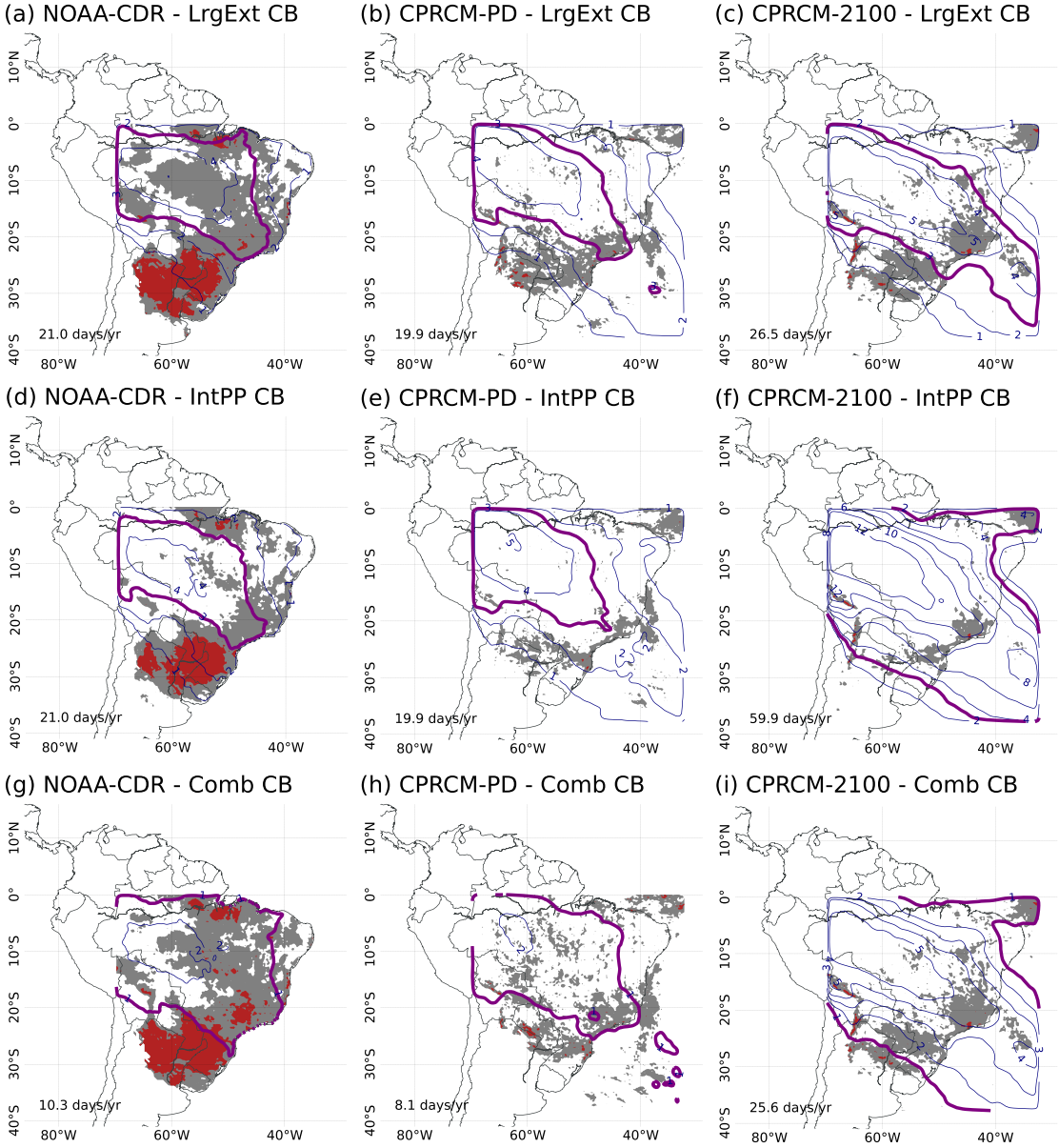

Figure 6. Percentage of days (blue contours every 1%, except in (f) every 2%) with large extent (first row), intense precipitation (second row), and combined (third row) cloud band events per year considering CHIRPS (first column), CPRCM-PD (second column) and CPRCM-2100 (third column). Thick magenta contour delimits the region where intense cloud band events are present in 3% (1% for combined CB events in the third row) of the days. Grey (red) shading indicates the areas with more than 20% (50%) of the intense cloud band days with precipitation above the PP95.

CB events over the study area; however, the CPRCM-PD simulation does overestimate the IntPPCB likelihood over the Amazon by ∼25% (figure 6, middle column). The CPRCM-PD also simulates the clusters of intense precipitation over eastern Brazil and SESA, albeit with underestimates of their frequency (shading in figure 6, middle column).

The future increase in the frequency of days with intense cloud bands is spatially uniform over the domain regardless of the intense cloud band category (figure 6, third column). The large increase in the frequency of IntPPCB is projected to result in their presence in more than 3% of the days (i.e. more than 11 d per year) in most of the study region (magenta contour in figure 6(f)) and will represent more than 10% of the days (i.e. more than 36 d per year) along the SACZ. The fraction of cloud band days with clusters of intense precipitation will also increase in this SACZ region (grey shades in figure 6(f)), particularly over coastal Southeastern Brazil, which hosts densely populated cities.

5. Discussion

Unprecedented rainfall extremes are being recorded more frequently each year across the globe (Robinson

et al 2021, Zhou *et al* 2022). South America is one of the regions already experiencing devastating extremes associated with rainfall intensification (Célia dos Santos Alvalá *et al* 2024, Marengo *et al* 2024). The large-scale circulation dynamics that give rise to tropical-extratropical cloud band events over South America (Zilli and Hart 2021) support regional intensification of rainfall relative to background rain rates in both observations and models (Zilli *et al* 2024). Here we show that under future warming, three metrics of area-averaged rain rates within these cloud bands increase (figure 3). These increases are greatest in CPRCM simulations, where the 95th percentile of cloud band-averaged rainfall increases by 26% (figure 3(a)). If scaled by the regional mean surface temperature increase of 5.7 K in CPRCM-2100, this equates to 4.5% K^{-1}. These values are obtained by spatially averaging the daily rain rates over the cloud band signature. Observational and modelling studies demonstrate that scaling greater than the CC relationship of ∼7% K^{-1} is often observed at rainfall stations or grid-points, particularly for sub-daily rainfall intensities (Lenderink and van Meijgaard 2008, Lenderink *et al* 2019, Fowler *et al* 2021). Given the spatial and temporal averaging adopted, short-duration extremes embedded into the future cloud bands will likely be even greater than the scaling reported here. Future work with additional convective-scale climate simulations should explore this risk further.

Kahana *et al* (2024) reported on all grid-point 3 h rainfall across South America in the CPRCM-2100 simulations and showed the same sign of change with a shift towards more intense rainfall. However, whether the CPRCM produced greater intensification than the parametrised-convection parent GCM was region-dependent. The results presented here focus on intensification during cloud bands under large-scale forcing, with the CPRCM simulation showing the greatest intensification, consistent with the review in Lenderink *et al* (2024).

To diagnose the absolute change in the probability of high-risk cloud bands in the future, we defined intense cloud band days by the extent and intensity of heavily raining regions embedded within the cloud band structures. In the present-day climate, intense cloud bands occur about 30 d (9% of the days) per year and are mainly located along the SACZ (3% of the days). Over SESA, the intense events are less frequent but are characterised by more intense precipitation (figure 6). In a high-emissions end-of-century scenario, the absolute number of days with intense CB triples, particularly those related to intense precipitation (IntPPCB, figure 4(d)), reflecting the precipitation intensification resulting from atmospheric warming. This increase occurs despite fewer cloud band days. In terms of probabilities, the chance of a 1-in-5 intense cloud band day at present could become a 3-in-5 chance in the future.

While these changes are strongest in the core austral summer months, an increase in the number of days with very intense cloud band systems is seen as late as May. In May 2024, massive floods were registered in South Brazil in the Rio Grande do Sul state, with circulation anomalies similar to those observed during a cloud band event (Batista Ferreira Neto 2024). This event aligns closely with the results described here showing that cloud band days with clusters of intense precipitation will become more frequent in this region (figures 5(b) and (c)) under warming. This increased risk in southeastern regions corroborates all-cause rainfall intensification reported in Kahana *et al* (2024). This event is a high-impact example of the growing risk of intense cloud band rainfall over South America under warming, increasing the likelihood of flash floods and landslides and unprecedented river catchment-scale flooding.

Data availability statement

The data that support the findings of this study are available upon reasonable request from the authors Ron Kahana or Kate Halladay.

Acknowledgments

This work and its contributors were supported by the Newton Fund through the Met Office Climate Science for Service Partnership Brazil (CSSP Brazil). M T Z and N C G H were also supported by a UKRI Future Leaders Fellowship MR/W011379/1. The authors would also like to acknowledge the valuable suggestions of the anonymous reviewers which improved the clarity of this paper.

ORCID iDs

Marcia T Zilli https://orcid.org/0000-0003-1670-8567
Neil C G Hart https://orcid.org/0000-0002-6902-8699
Kate Halladay https://orcid.org/0000-0002-1195-4497
Ron Kahana https://orcid.org/0000-0003-2070-8818

References

Andrews M B *et al* 2020 Historical simulations with HadGEM3-GC3.1 for CMIP6 *J. Adv. Model. Earth Syst.* **12** 1–34
Batista Ferreira Neto J 2024 Impact of April and May 2024 extreme precipitation on flooding in Rio Grande Do Sul,

Brazil: an integrated analysis (available at: https://papers.ssrn.com/abstract = 4922295)
Berthou S, Rowell D P, Kendon E J, Roberts M J, Stratton R A, Crook J A and Wilcox C 2019 Improved climatological precipitation characteristics over West Africa at convection-permitting scales *Clim. Dyn.* **53** 1991–2011
Célia dos Santos Alvalá R, Ribeiro D F, Marengo J A, Seluchi M E, Gonçalves D A, Antunes da Silva L, Cuartas Pineda L A and Saito S M 2024 Analysis of the hydrological disaster occurred in the state of Rio Grande do Sul, Brazil in September 2023: vulnerabilities and risk management capabilities *Int. J. Disaster Risk Reduct.* **110** 104645
Coelho C A S *et al* 2016 The 2014 Southeast Brazil austral summer drought: regional scale mechanisms and teleconnections *Clim. Dyn.* **46** 3737–52
Crook J, Klein C, Folwell S, Taylor C M, Parker D J, Stratton R and Stein T 2019 Assessment of the representation of West African storm lifecycles in convection-permitting simulations *Earth Space Sci.* **6** 818–35
da Fonseca Aguiar L and Cataldi M 2021 Social and environmental vulnerability in Southeast Brazil associated with the South Atlantic convergence zone *Nat. Hazards* **109** 2423–37
Fowler H J *et al* 2021 Anthropogenic intensification of short-duration rainfall extremes *Nat. Rev. Earth Environ.* **2** 107–22
Funk C *et al* 2015 The climate hazards infrared precipitation with stations—a new environmental record for monitoring extremes *Sci. Data* **2** 1–21
Halladay K, Kahana R, Johnson B, Still C, Fosser G and Alves L 2023 Convection-permitting climate simulations for South America with the Met Office unified model *Clim. Dyn.* **1** 1–23
Hart N C G, Reason C J C and Fauchereau N 2012 Building a tropical–extratropical cloud band metbot *Mon. Weather Rev.* **140** 4005–16
Hersbach H *et al* 2020 The ERA5 global reanalysis *Q. J. R. Meteorol. Soc.* **146** 1999–2049
Kahana R, Halladay K, Alves L M, Chadwick R and Hartley A J 2024 Future precipitation projections for Brazil and tropical South America from a convection-permitting climate simulation *Front. Clim.* **6** 141970
Kendon E J, Stratton R A, Tucker S, Marsham J H, Berthou S, Rowell D P and Senior C A 2019 Enhanced future changes in wet and dry extremes over Africa at convection-permitting scale *Nat. Commun.* **10** 1–14
Knapp K R 2008 Scientific data stewardship of international satellite cloud climatology project B1 global geostationary observations *J. Appl. Remote Sens.* **2** 023548
Kuhlbrodt T *et al* 2018 The low-resolution version of HadGEM3 GC3.1: development and evaluation for global climate *J. Adv. Model. Earth Syst.* **10** 2865–88
Lee D, Min S K, Park I H, Ahn J B, Cha D H, Chang E C and Byun Y H 2022 Enhanced role of convection in future hourly rainfall extremes over South Korea *Geophys. Res. Lett.* **49** e2022GL099727
Lee H-T 2014 Climate algorithm theoretical basis document (C-ATBD): outgoing longwave radiation (OLR)—daily (available at: www1.ncdc.noaa.gov/pub/data/sds/cdr/CDRs/Outgoing%20Longwave%20Radiation%20-%20Daily/AlgorithmDescription_01B-21.pdf) (Accessed 6 November 2019)
Lee H-T (NOAA-CDR Program) 2011 *NOAA Climate Data Record (CDR) of Daily Outgoing Longwave Radiation (OLR), Version 1.2* (https://doi.org/10.7289/V5SJ1HH2)
Lenderink G, Ban N, Brisson E, Berthou S, Cortés-Hernández V E, Kendon E, Fowler H and de Vries H 2024 Are dependencies of extreme rainfall on humidity more reliable in convection-permitting climate models? *Hydrol. Earth Syst. Sci. Discuss.* **29** 1201–20
Lenderink G, Belušić D, Fowler H J, Kjellström E, Lind P, Meijgaard E v, Ulft B V and Vries H d 2019 Systematic increases in the thermodynamic response of hourly precipitation extremes in an idealized warming experiment with a convection-permitting climate model *Environ. Res. Lett.* **14** 074012
Lenderink G and van Meijgaard E 2008 Increase in hourly precipitation extremes beyond expectations from temperature changes *Nat. Geosci.* **1** 511–4
Marengo J A *et al* 2024 Heavy rains and hydrogeological disasters on February 18th–19th, 2023, in the city of São Sebastião, São Paulo, Brazil: from meteorological causes to early warnings *Nat. Hazards* **120** 7997–8024
Monerie P-A, Chevuturi A, Cook P, Klingaman N P and Holloway C E 2020 Role of atmospheric horizontal resolution in simulating tropical and subtropical South American precipitation in HadGEM3-GC31 *Geosci. Model Dev.* **13** 4749–71
Prein A, Gobiet A, Suklitsch M, Truhetz H, Awan N, Keuler K and Georgievski G 2013 Added value of convection permitting seasonal simulations *Clim. Dyn.* **41** 2655–77
Reynolds R W, Smith T M, Liu C, Chelton D B, Casey K S and Schlax M G 2007 Daily high-resolution-blended analyses for sea surface temperature *J. Clim.* **20** 5473–96
Robinson A, Lehmann J, Barriopedro D, Rahmstorf S and Coumou D 2021 Increasing heat and rainfall extremes now far outside the historical climate *npj Clim. Atmos. Sci.* **4** 1–4
Williams K D *et al* 2018 The Met Office global coupled model 3.0 and 3.1 (GC3.0 and GC3.1) configurations *J. Adv. Model. Earth Syst.* **10** 357–80
Xavier A C, Scanlon B R, King C W and Alves A I 2022 New improved Brazilian daily weather gridded data (1961–2020) *Int. J. Climatol.* **42** 8390–404
Zhou T, Zhang W, Zhang L, Clark R, Qian C, Zhang Q, Qiu H, Jiang J and Zhang X 2022 2021: a year of unprecedented climate extremes in Eastern Asia, North America and Europe *Adv. Atmos. Sci.* **39** 1598–607
Zilli M T and Hart N C G 2021 Rossby wave dynamics over South America explored with automatic tropical–extratropical cloud band identification framework *J. Clim.* **34** 8125–44
Zilli M T, Hart N C G, Coelho C A S, Chadwick R, de Souza D C, Kubota P Y, Figueroa S N and Cavalcanti I F A 2023 Characteristics of tropical–extratropical cloud bands over tropical and subtropical South America simulated by BAM-1.2 and HadGEM3-GC3.1 *Q. J. R. Meteorol. Soc.* **149** 1498–519
Zilli M T, Lemes M R, Hart N C G, Halladay K, Kahana R, Fisch G, Prein A, Ikeda K and Liu C 2024 The added value of using convective-permitting regional climate model simulations to represent cloud band events over South America *Clim. Dyn.* **62** 10543–64